



Publication Year	2020
Acceptance in OA	2022-02-18T14:45:08Z
Title	Multidisciplinary Analysis of Lermontov Crater on Mercury
Authors	PAJOLA, MAURIZIO, LUCCHETTI, ALICE, Semenzato, A., Munaretto, G., POGGIALI, GIOVANNI, GALLUZZI, VALENTINA, CREMONESE, Gabriele, BRUCATO, John Robert, Palumbo, P., Massironi, M.
Handle	http://hdl.handle.net/20.500.12386/31417

MULTIDISCIPLINARY ANALYSIS OF LERMONTOV CRATER ON MERCURY. Maurizio Pajola¹, A. Lucchetti¹, A. Semenzato², G. Munaretto^{1,3}, G. Poggiali^{4,5}, V. Galluzzi⁶, G. Cremonese¹, J.R. Brucato⁴, P. Palumbo⁷, M. Massironi². ¹INAF-Astronomical Observatory of Padova, Vicolo dell'Osservatorio 5, 35122 Padova, Italy (maurizio.pajola@inaf.it); ²Geosciences Dept., University of Padova, Italy; ³Department of Physics and Astronomy "G. Galilei", University of Padova, Padova, Italy; ⁴INAF-Astrophysical Observatory of Arcetri, Firenze, Italy; ⁵Università degli Studi di Firenze, Firenze, Italy; ⁶INAF-IAPS Roma, Istituto di Astrofisica e Planetologia Spaziali di Roma, Rome, Italy; ⁷DiST-Utiversità degli Studi di Napoli "Parthenope", Napoli, Italy.

Introduction: The Lermontov crater is a 166-km size crater located at 15.24°N, 48.94°W in the Kuiper quadrangle of Mercury. This crater was first identified in Mariner 10 images thanks to its particularly bright floor characterized by smooth plains [1]. A first possible explanation for this brightness behavior was given by [2], suggesting that it is the result of fumarolic alteration along floor fractures. Nevertheless, since the crater floor appears to have a lower crater density than the surroundings and its northeast part has irregular rimless pits (this is indicative of endogenic modification) [3,4] proposed that the bright floor deposit might have been emplaced by pyroclastic activity. By means of MESSENGER flybys 1-3 images, [5] eventually identified Lermontov floor deposit as one of the 35 pyroclastic deposits observed on Mercury. In particular, the pit associated with the Lermontov NE pyroclastic deposit is morphologically similar to the one associated with the lunar pyroclastic deposit Sulpicius Gallus [6,7], where a non-circular shape, rimless margins and lack of ejecta deposits is evident. In this work, we analyze the Lermontov crater performing a high-resolution geological map and determining the modelled age. In addition, through a well-developed methodology we spectrophotometrically study the Lermontov crater in order to determine its compositional behavior and find if there are any correlation and/or differences between the identified geological units, such as hollows and pyroclastic deposits.

Geological map: In this multidisciplinary work we use the MESSENGER-Mercury Dual Imaging System Narrow Angle Camera (MDIS-NAC, [8]) 35 m-scale images to prepare the first high-resolution geological map of the crater and its closes surroundings (Figure 1), distinguishing seven different units and four linear features. Among the several features identified, the crater floor appears strongly affected by hollow-related morphologies and deposits, which cover almost entirely the flat area inside the crater, and also some portions of the crater wall and ejecta (in the northern sector). Another important feature, identified within the crater floor, is an unnamed *facula* (i.e., a bright spot, usually attributed to pyroclastic deposits on Mercury, [5]), which covers almost entirely the crater

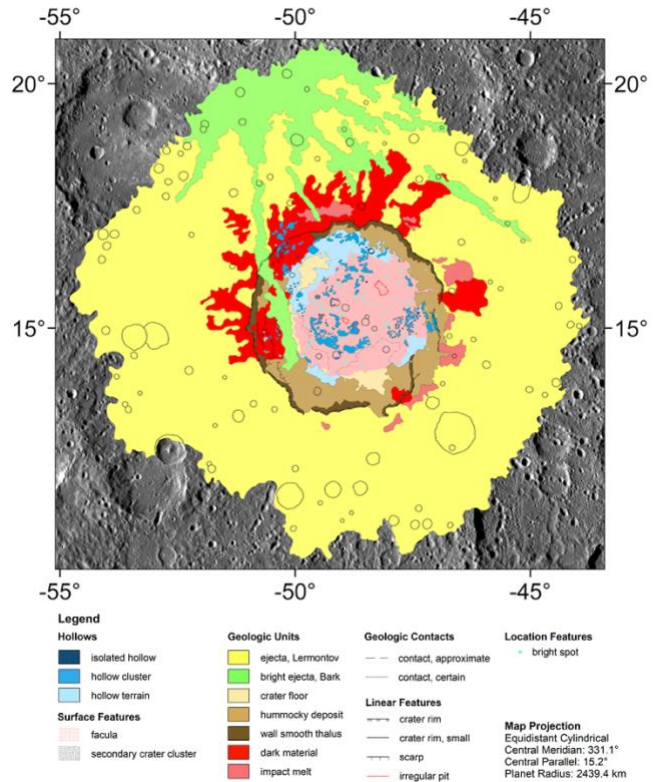


Figure 1: Geological map of Lermontov crater.

floor in the central and eastern portion, but it appears to be older than hollows deposits (that are found on top of the *facula*).

Age determination: Through the crater counting technique applied on the crater floor, the derived modelled age ranges between 3.84 and 3.74 Ga [9,10]. This age is older than the Mansurian one previously suggested for Lermontov [11], hence dating back the emplacement of the crater into the Calorian age.

Spectrophotometric analysis: On the photometrically corrected MDIS-Wide Angle Camera (WAC) multiband dataset (Figure 2, 266 m-scale), we apply an unsupervised spectral clustering K-means technique [12,13] that separates the different deposits located both inside and outside the Lermontov crater. This allows us to separate our studying area in clusters, each one characterized by an average multi-colour

spectrum and its associated variability. In addition, the relative geographical information of each spectrum is maintained in the process, allowing us to geolocate the cluster on the studied surface and investigate correlations with geographical surface features. Despite a coarser resolution of the WAC, when compared with the NAC, we clearly identify that the pyroclastic deposits located on the crater's floor have a steep, red spectral slope. On the contrary, the vents' rims are characterized by several hollows (well visible with inside the WAC images) whose spectral slope is bluer than the pyroclastic deposits themselves and the absorption bands are similar to those identified inside hollows located far away from the vents. Eventually, the mineralogical analysis of the derived spectra will be presented.

We underline that the Lermontov crater will be one of the main target that will be observed through the BepiColombo future SIMBIO-SYS instrument suite [14]. Such dataset will definitely allow a more detailed morphological and spectrophotometric analysis of this crater.

Acknowledgments: This activity has been realized under the BepiColombo ASI-INAF contract no 2017-47-H.0.

References: [1] DeHon, R. A., et al., (1981), *U.S. Geol. Surv. Misc. Invest. Ser. Map*, I-1233. [2] Dzurisin, D. (1977), *GRL*, 4(10), 383– 386. [3] Schultz, P. H. (1977), *Phys. Earth Planet. Inter.*, 15, 202–219. [4] Rava, B., and B. Hapke (1987), *Icarus*, 71, 397– 429. [5] Kerber, L. et al. (2011), *PSS*, 59, 1895–1909. [6] Lucchitta, B.K., Schmitt, H.H., (1974). *Proc. Lunar. Sci. Conf.* 5, 223–234. [7] Gaddis, L.R. et al. (2003, *Icarus* 161, 262–280. [8] Hawkins, S. E. et al. (2007), *Space Sci. Rev.*, 131(1–4), 247–338. [9] Neukum, G., et al., (2001b), *PSS*, 49, 1507–1521. [10] Le Feuvre M. and Wieczorek, M.A. (2011), *Icarus*, 214, 1-20. [11] Blewett, D. T., et al. (2013), *JGR*, 118. [12] Pajola, M. et al. (2018), *PSS*, 154, 63–71. [13] Lucchetti, A. et al. (2018), *JGR*, 123. [14] Cremonese, G. et al., *Space Sci. Rev.* (submitted).

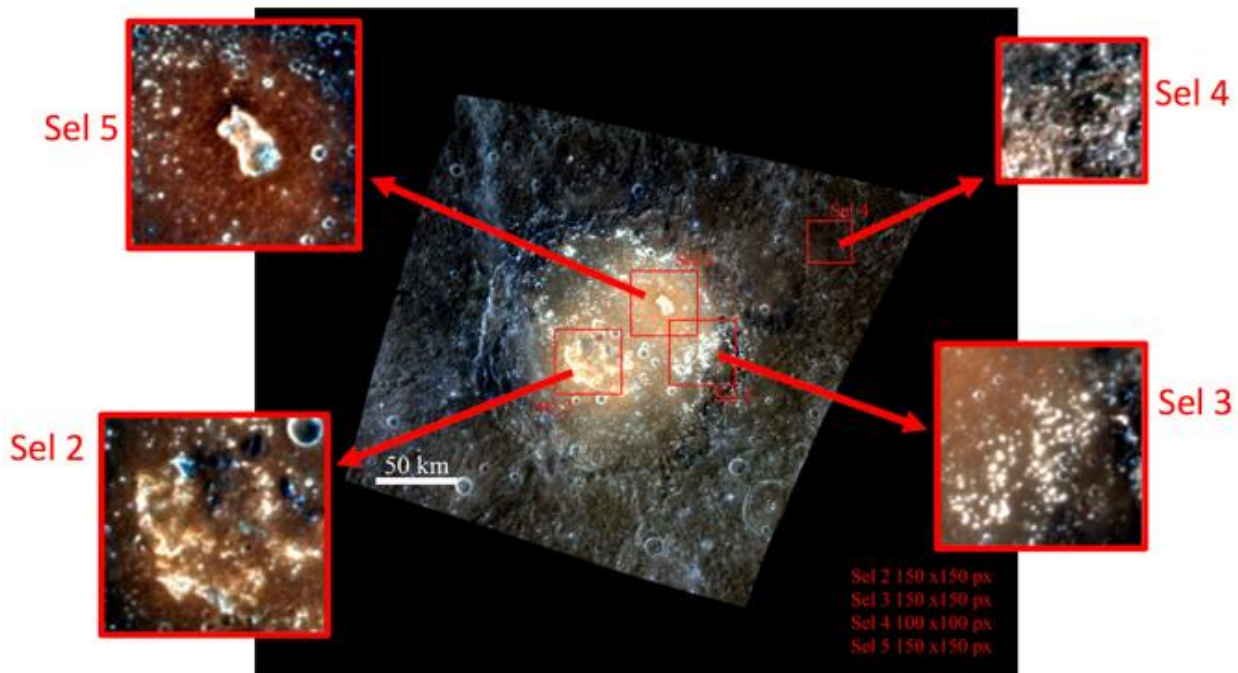


Figure 2: The MDIS WAC dataset where we applied the K-mean clustering algorithm. The four boxes represent the Region of Interest we studied.